buildings

MDPI

Article

Study on Wind-Induced Dynamic Response and Statistical Parameters of Skeleton Supported Saddle Membrane Structure in Arching and Vertical Direction

Ziye Chen [1], Changjiang Liu [1,2,*], Dong Li [3,*], Jian Liu [1,2], Xiaowei Deng [4], Chiyu Luo [5] and Guangen Zhou [2,6]

[1] School of Civil Engineering, Guangzhou University, Guangzhou 510006, China
[2] Guangdong Engineering Technology Research Center for Complex Steel Structures, Guangzhou University, Guangzhou 510006, China
[3] School of Civil Engineering, Fuzhou University, Fuzhou 350116, China
[4] Department of Civil Engineering, The University of Hong Kong, Pokfulam, Hong Kong 999077, China; xwdeng@hku.hk
[5] Architectural Design and Research Institute of Guangdong Province, Guangzhou 510000, China
[6] Zhejiang Southeast Space Frame Co., Ltd., Hangzhou 311209, China
* Correspondence: cjliu@gzhu.edu.cn (C.L.); dongli@fzu.edu.cn (D.L.)

Abstract: Wind tunnel tests and numerical simulations are the mainstream methods to study the wind-induced vibration of structures. However, few articles use statistical parameters to point out the differences and errors of these two research methods in exploring the wind-induced response of membrane structures. The displacement vibration of a saddle membrane structure under the action of wind load is studied by wind tunnel tests and numerical simulation, and statistical parameters (mean, range, skewness, and kurtosis) are introduced to analyze and compare the displacement data. The most unfavorable wind direction angle is 0° (arching direction). The error between experiment and simulation is less than 10%. The probability density curve has a good coincidence degree. Both the test and simulation show a certain skewed distribution, indicating that the wind-induced vibration of the membrane does not obey the Gaussian distribution. The displacement response obtained by the test has good stability, while the simulated displacement response has strong discreteness. The difference between the two research methods is quantitatively given by introducing statistical parameters, which is helpful to improve the shortcomings of wind tunnel tests and numerical simulations.

Keywords: wind tunnel test; numerical simulation; saddle membrane structure; wind-induced dynamic response; statistical parameter

Citation: Chen, Z.; Liu, C.; Li, D.; Liu, J.; Deng, X.; Luo, C.; Zhou, G. Study on Wind-Induced Dynamic Response and Statistical Parameters of Skeleton Supported Saddle Membrane Structure in Arching and Vertical Direction. *Buildings* **2024**, *14*, 1339. https://doi.org/10.3390/buildings14051339

Academic Editor: Pedro Martinez-Vazquez

Received: 20 March 2024
Revised: 30 April 2024
Accepted: 3 May 2024
Published: 9 May 2024

1. Introduction

The membrane structure is mainly composed of the membrane material and the skeleton that plays a supporting and fixing role. It has the advantages of lightweight, high tensile strength, and good seismic performance [1,2]. Because of its unique performance, it can ensure a large rise–span ratio. It is often designed into various negative Gaussian curvature spatial shapes [3–5], which is very ornamental and widely used in modern large-span spatial structures. The structure will be affected by wind load, rain load, and hail impact load in daily use [6–9]. For example, Cui et al. [10] established a reduced-order modeling procedure to simulate the wind-induced buffeting vibration of long-span bridges. At the same time, they used the Fokker–Planck–Kolmogorov equation to exam the occurrence probability of vortex-induced vibration on long-span bridge decks [11]. Jacome et al. [12] optimized the aerodynamic-induced vibration of the wing based on the uncertainty-based aerodynamic optimization method. Scholars at home and abroad have also carried out related research on steel structures [13], high-rise buildings [14–16] and other building structures [17–23].

However, the scope of the above research is a rigid structure, and less research has investigated flexible structures. The membrane structure, as a classical flexible structure, has a large deformation amplitude under the action of wind load, and the membrane even undergoes tearing damage under extreme conditions [24–27]. Studying and calculating the displacement response of the membrane structure under different conditions can intuitively understand the effect and influence of wind on the structure. Chen et al. [28] explored the interference effects of wind load and wind-induced responses of parallel-arranged rectangular-planed air-supported membrane structures through wind tunnel tests. He et al. [29] used ANSYS software to explore the influence of different cable-membrane connection models on the wind-induced response of the air-supported membrane structure with an orthogonal cable net. At the same time, the introduction of appropriate statistical parameters is helpful to analyze the distribution law of the wind-induced displacement response of structures and then take effective measures and methods to reduce the displacement vibration. Zhang et al. [30] established the finite element model of the transmission tower-line system by ANSYS software, and they statistically analyzed the wind-induced dynamic response.

At present, the mainstream research methods of random vibration of membrane structures under the action of wind load include theoretical formulas, actual measurements, wind tunnel tests and numerical simulation. Among them, the theoretical formula introduces more assumptions when establishing the equation, ignoring important factors such as fluid–solid coupling, so there is a certain error between the calculation results and the actual situation. The financial and human resources spent on the actual measurement are too much, and the final effect can only help the next maintenance; it cannot provide some reference for the construction in advance. However, the wind tunnel test only needs to consider the similarity criterion and can accurately restore the wind field characteristics, which is valued by scholars at home and abroad. Chen et al. [31] carried out wind tunnel tests on the aeroelastic model of an open one-way tensioned membrane, and they studied the aeroelastic instability mechanism of the membrane structure. Wood et al. [32] used wind tunnel tests to study the fluid–solid coupling of flexible hemisphere-shaped membrane structures, and they analyzed the comprehensive data set of fluid flow and structural displacement. With the rapid development of computers, computational fluid dynamics is widely used in numerical simulation [33–35]. Its low cost, short cycle and strong repeatability have made it a popular research method. Kawulok et al. [36] used RFEM software to numerically analyze the wind flow and simulated the wind tunnel in RWIND software. Sun et al. [37] used the large eddy simulation method to explore the wind pressure characteristics of large-span roofs under vertical wind direction fluctuations. In addition, they also studied the effects of wind-induced vibration response and wind pressure distribution on saddle, wavy and continuous arched roofs.

Although there are various research methods [38–41], each with its own application scope and advantages, there are also some limitations to these methods. The wind tunnel test uses the similarity theory but relaxes the requirements of some physical parameters, and the real situation of the membrane structure cannot be completely restored during the test. The numerical simulation uses the turbulence model to simplify the Navier–Stokes equation, and the calculation accuracy is affected by the turbulence model. However, few scholars and teams have calculated the error of the wind tunnel test and numerical simulation in studying the wind-induced response of saddle membrane structures under the action of wind load. At the same time, few research papers have applied statistical knowledge to point out the differences between the two research methods. The results of the study can be used to train machine learning [42–45] and artificial intelligence algorithms [46–48], and these effective algorithms in turn contribute to the optimization and design of membrane structures. The saddle is one of the most common forms of modern membrane structures, but it has a special shape. When conducting random vibration analysis, it is necessary to consider the influence of wind loads at different wind directions on the membrane structure, so it is the preferred research object.

Taking the skeleton-supported saddle membrane structure as an example, the wind-induced dynamic response of the skeleton-supported saddle membrane structure under the action of wind load is studied by wind tunnel tests and finite element numerical simulations. The displacement response and wind pressure distribution of the membrane structure at different wind direction angles (arching or vertical direction) are explored, and the absolute error and relative error of the two research methods are discussed. The novel aspect is the introduction of statistical parameters (skewness and kurtosis), and the reasons for the different shapes and offsets of the curves are elaborated from the perspective of probability density. The differences between wind tunnel tests and numerical simulations in studying the wind-induced response of saddle membrane structures are analyzed, which is conducive to the subsequent correction of numerical simulation methods. The technical route is shown in Figure 1.

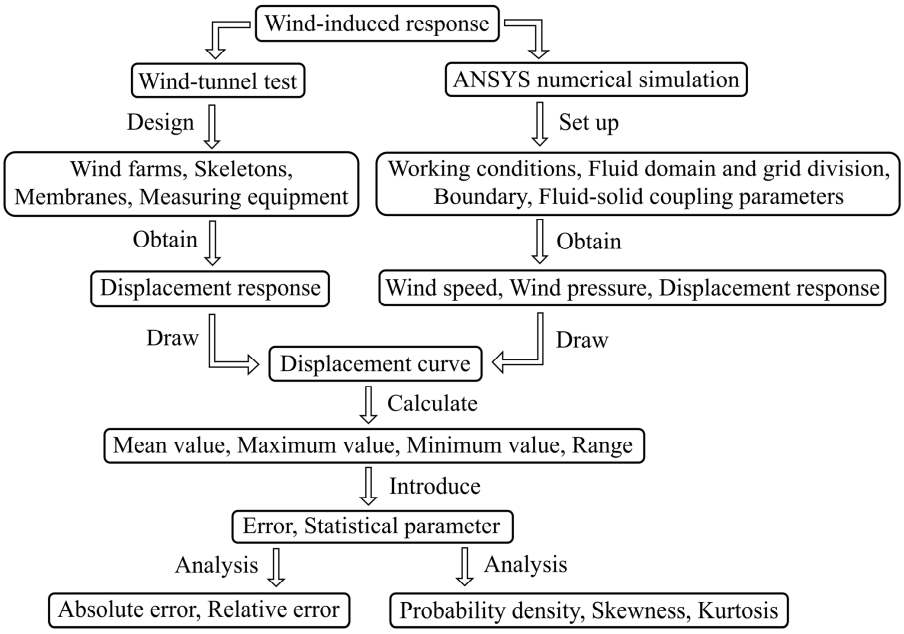

Figure 1. Technical route.

2. Wind Tunnel Tests

The wind tunnel tests can well restore and reflect the load size and vibration of the membrane structure in the actual use process [49,50]. In order to reduce the error caused by the similarity ratio conversion process of physical parameters and keep the same parameters with the model of numerical simulation below, the similarity theory is not considered in the wind tunnel test.

2.1. Test Models and Equipment

2.1.1. Wind Tunnel Site

The wind tunnel is an annular reflux type, and the wind tunnel structure diagram is shown in Figure 2. At the same time, a large number of cube roughness elements are set up inside the wind tunnel to simulate the roughness of the ground. The gradient wind speed and turbulence intensity required for the test can be obtained by changing the arrangement. The test layout inside the wind tunnel is shown in Figure 3.

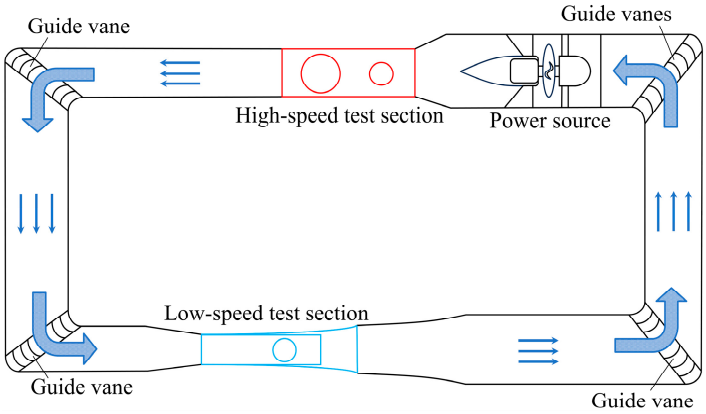

Figure 2. Wind tunnel structure diagram.

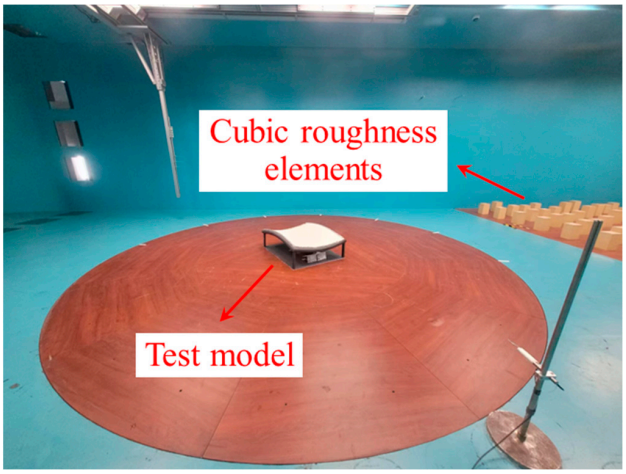

Figure 3. Wind tunnel internal test layout.

2.1.2. Test Membrane Material

The membrane material used for the tests is rainproof silk fabric, and the size of the membrane is a square with a side length of 1 m, as shown in Figure 4. Other physical parameters of the membrane are provided by the manufacturer, as shown in Table 1. *Ex* and *Ey* represent the modulus of elasticity in the *x* and *y* directions, respectively.

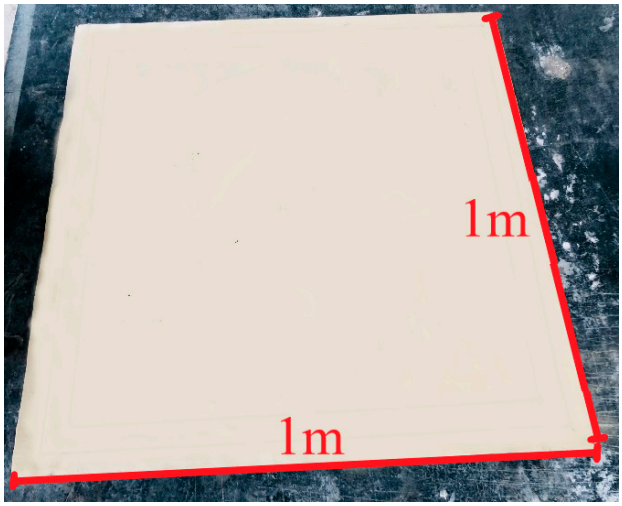

Figure 4. Test membrane material.

Table 1. Mechanical property parameters of test membrane.

Parameter (Unit)	Value
Areal density (kg/m^2)	0.64
Thickness (mm)	1
Poisson ratio	0.4
Elastic modulus (*Ex* and *Ey*) (kN/m^2)	5×10^4

2.1.3. Model Skeleton

The design prototype of the skeleton-supported membrane structure's model skeleton comes from the actual engineering membrane structure. According to the boundary of the actual project, it is simply supported on four sides. The size of the skeleton and the boundary support technique are the key characteristics that affect the dynamic response of the membrane structure. The model skeleton of the test is composed of four short straight steel tubes, which are spliced by the upper four bending steel tubes and the bottom light steel plate. The vertical projection is a square with a side length of 1.0 m. The heights of the four corner points are all 0.3 m, the spans are 1/8 in both the arch direction and the vertical direction, and the schematic diagram of the model skeleton is shown in Figure 5. The actual project size can be obtained by similarity ratio conversion. The length similarity ratio between the prototype and the model is 10:1, so the size of the actual membrane structure project is 10 m × 10 m.

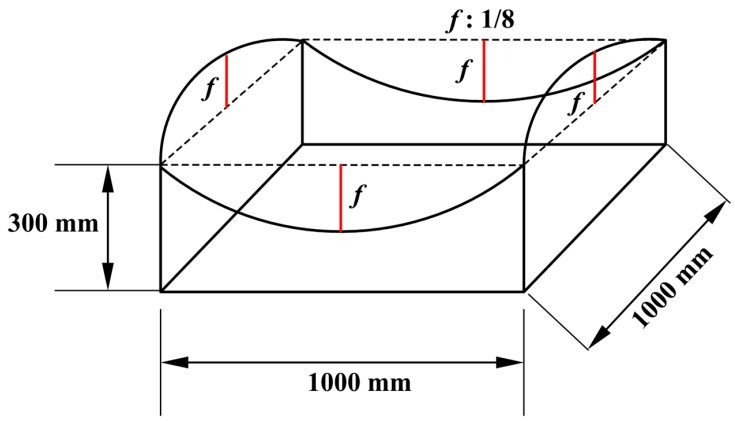

Figure 5. Model skeleton.

The test membrane material is installed on the model skeleton. The edges of the membrane are fully clamped. In order to accurately control the magnitude of the pretension applied before the installation of the membrane material, the ANSYS finite element software is used to find the form-finding analysis of the membrane material. It can be seen from Figure 6 that the stress of the membrane is stable at about 2500 Pa. The dynamometer is repeatedly stretched and fixed on the curved steel pipe of the model skeleton with rivets.

2.1.4. Data Acquisition Device

The laser displacement sensor is used to obtain the vibration of the membrane, as shown in Figure 7. The displacement data of the membrane can be measured by adjusting the laser emitter of the sensor to the monitoring point on the membrane. The wind speed data are obtained by the wind speed measuring instrument, as shown in Figure 8. The wind speed measuring instrument is placed 20 cm above the center point of the membrane, and the wind speed data above the membrane can be monitored.

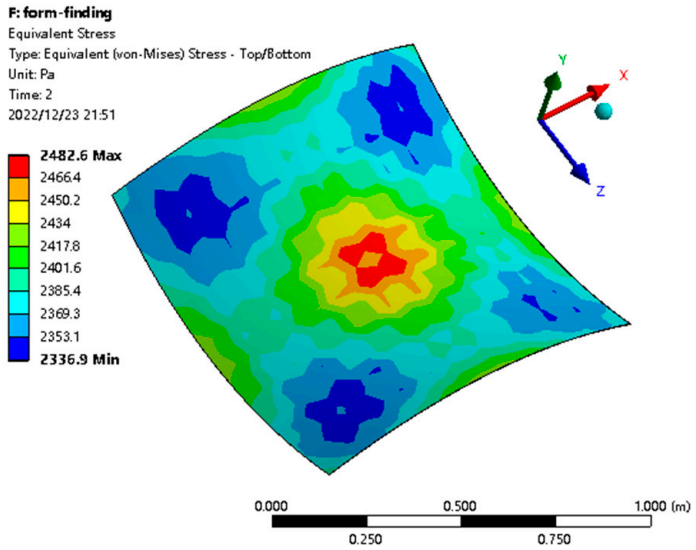

Figure 6. Form-finding stress diagram.

Figure 7. Laser displacement sensor.

Figure 8. Wind speed measuring instrument.

2.2. Test Procedure

2.2.1. Wind Field Characteristics

The class B ground roughness (hills and townships with relatively sparse houses) of the Chinese building structure load code is selected as the test condition. Before the formal test, the arrangement of the ground roughness elements is continuously adjusted to meet the wind field characteristics corresponding to the class B ground roughness. It can be seen from Figure 9 that the wind field characteristics required for the test well meet

the requirements of wind speed profile and turbulence intensity (Equations (1) and (2)). The Davenport wind spectrum is representative due to its simplicity of definition. The conservative assumptions of the Davenport wind speed spectrum are also taken into account, so the Davenport wind speed spectrum is adopted. It can also be seen from Figure 10 that the fluctuating wind speed spectrum of the wind tunnel test satisfies the Davenport spectrum (Equation (3)), so the test wind field satisfies the required atmospheric boundary layer. The turbulence integral scale is a measure of the average vortex size in the airflow. The estimation results of the turbulence scale mainly depend on the length of the records used in the estimation analysis and the smoothness of the records. Different experiments generally differ significantly. Therefore, this feature is not considered.

$$V = 12(h/0.3)^{0.15} \tag{1}$$

$$I = 0.14(h/10)^{-0.15} \tag{2}$$

$$\frac{f \cdot S_u(f)}{u_*^2} = \frac{4\overline{f}^2}{(1+\overline{f}^2)^{\frac{4}{3}}} \tag{3}$$

where V represents wind speed; h represents height from the ground; I represents turbulence intensity. $S_u(f)$ represents wind speed spectrum; u_* represents the flow shear velocity; $\overline{f} = (fL)/V_{10}$; f represents the frequency of fluctuating wind; L = 1200 m; V_{10} indicates the wind speed at a height of 10 m.

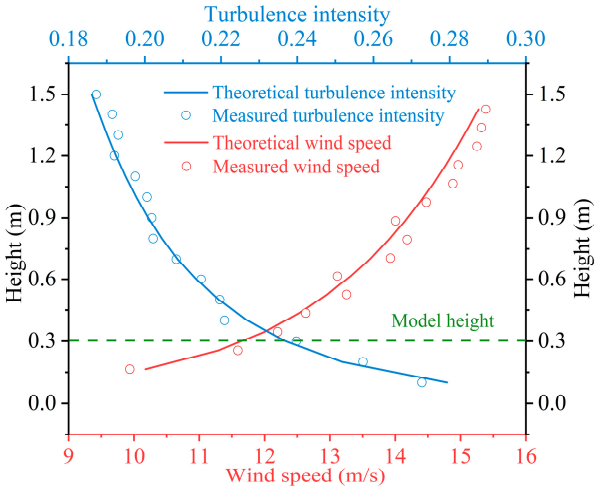

Figure 9. Wind speed profile and turbulence intensity.

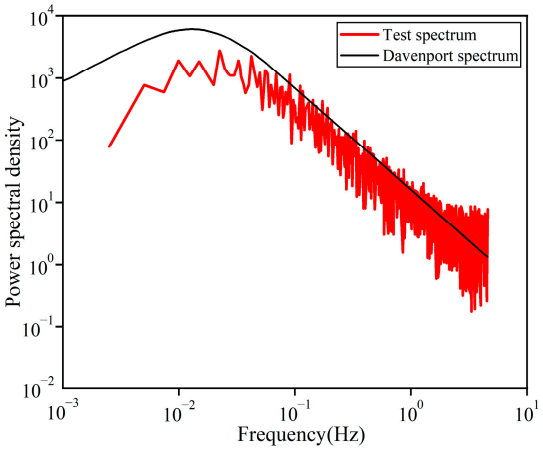

Figure 10. Power density spectrum.

2.2.2. Test Conditions and Schemes

The membrane material is trimmed with rain-proof silk cloth. At the same time, the marker pen is used to mark seven monitoring points on the intersection of the vertical and horizontal lines of the membrane material. The specific layout is shown in Figure 11.

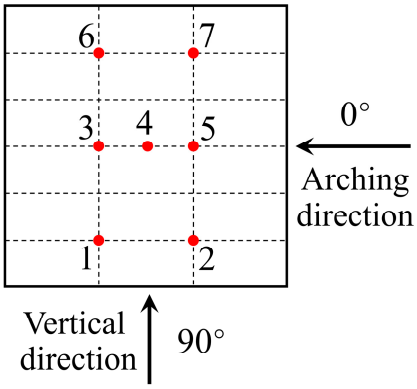

Figure 11. Layout of monitoring points on membrane.

In this test, 0° (arching direction) and 90° (vertical direction) wind direction angle blowing model structures are set up. The target wind speed is adjusted, and the response signal is collected after the wind speed and the membrane vibration are stabilized. This stage is the steady-state response data of the membrane.

2.3. Test Result Analysis

In this test, seven monitoring points are marked on the membrane, which can better observe the change in displacement of each point and reveal the wind-induced dynamic response law of membrane structure for us. However, due to the large amount of data collected, we only show the vibration of two monitoring points, and the displacement response of the remaining points only shows the mean and extreme values (maximum positive values and minimum negative values).

Point 2 is a monitoring point on the windward surface of different wind direction angles, which is worthy of attention and discussion. At the same time, considering that the center point 4 of the membrane is the farthest from the edge of the model skeleton, the binding force is the smallest, and the vibration amplitude of the membrane is the largest. Therefore, this point is the most noteworthy monitoring point, which should be analyzed and discussed. Therefore, the displacement response curves of monitoring points 2 and 4 at 0° and 90° wind direction angles are given. At the same time, the mean displacement and the range of displacement change are indicated in each diagram, as shown in Figure 12.

The data set is processed, and the time of 0 s is not the starting point of the test but rather the starting point of the steady-state vibration of the membrane. Since the laser displacement sensor is installed below the membrane, when the displacement response is negative, it indicates that the membrane is far away from the laser displacement sensor, which represents the upward movement of the membrane. Conversely, it means that the membrane moves downward. It can be seen from the group diagram 12 that the steady-state vibration of the membrane is characterized by irregular vibration at a new equilibrium position deviating from the initial state, whether it is under the action of a 0° or 90° wind angle.

For the sake of brevity, only the dynamic displacements of points 2 and 4 have been presented. The displacement response of the remaining monitoring points is similar to that of points 2 and 4, and the membrane is also irregularly vibrated near the mean value. The mean value can represent the characteristics of the overall data, and it can also intuitively describe the central trend of the data. At the same time, to further understand the stability of the data, the maximum positive values and minimum negative values can be introduced on the basis of the mean value. In the dynamic response analysis, the statistical parameters

of the membrane can better reflect the vibration law, focusing on the mean and extreme values of displacement. In order to obtain accurate statistical data as much as possible and reduce the randomness and uncertainty in the wind tunnel test process, the displacement mean and displacement extreme value of 30 s in the steady-state stage are calculated. Table 2 shows the mean displacement of each monitoring point at 0° and 90° wind direction angles in the wind tunnel test. Table 3 shows the displacement extreme values of each monitoring point under 0° and 90° wind direction angles in the wind tunnel test.

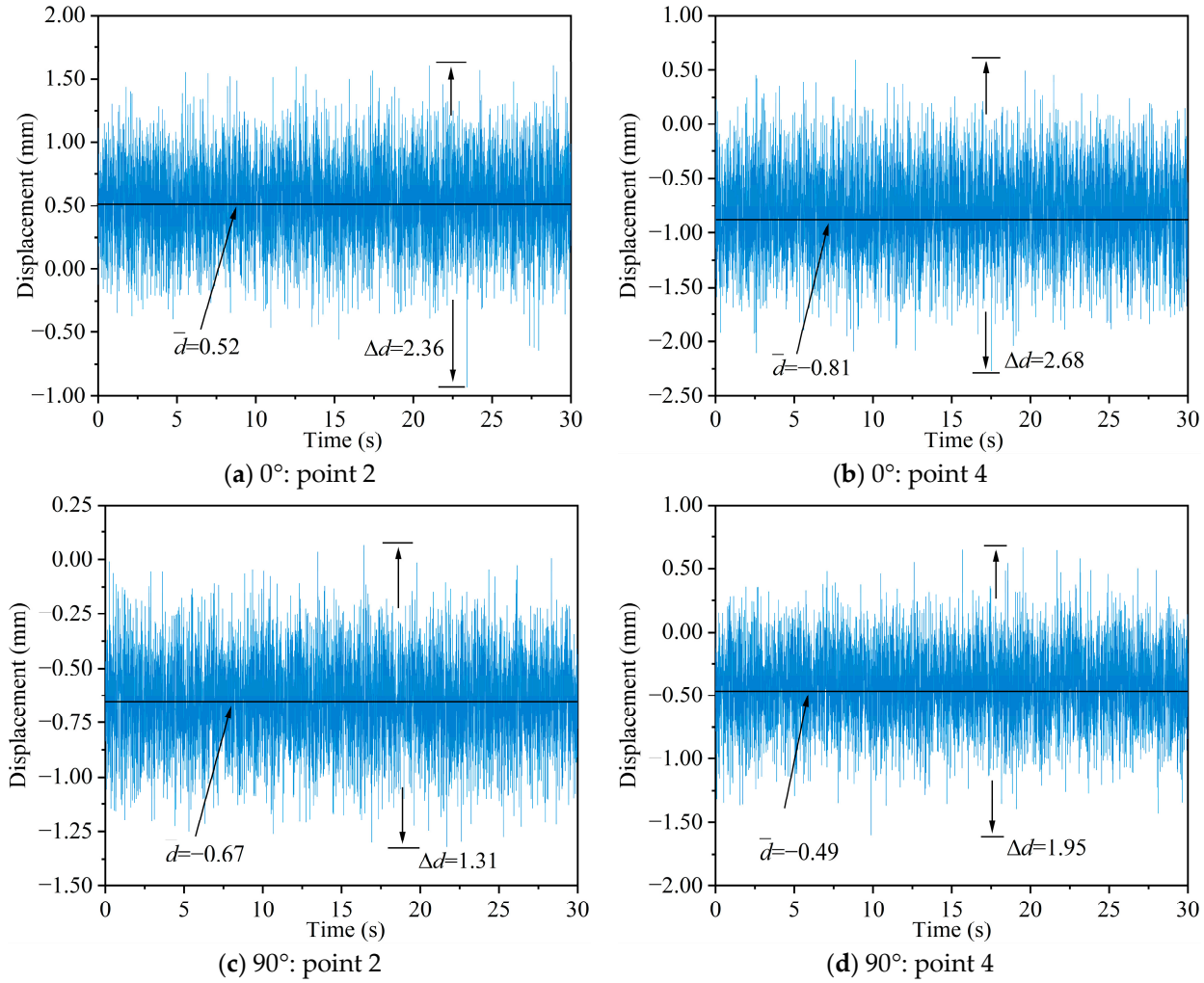

(**a**) 0°: point 2 (**b**) 0°: point 4

(**c**) 90°: point 2 (**d**) 90°: point 4

Figure 12. Displacement response curve under wind tunnel test.

Table 2. The mean displacement of each point under wind tunnel test (mm).

Wind Direction Angle: Displacement	Point 1	Point 2	Point 3	Point 4	Point 5	Point 6	Point 7
0°	−0.42	0.52	−0.76	−0.81	0.58	−0.61	0.51
90°	−0.56	−0.67	−0.41	−0.49	−0.64	0.32	0.28

Table 3. The displacement extreme value of each point under wind tunnel test (mm).

Wind Direction Angle: Displacement	Point 1	Point 2	Point 3	Point 4	Point 5	Point 6	Point 7
0°: maximum positive values	0.45	1.55	0.52	0.53	1.62	0.39	1.72
90°: maximum positive values	0.12	0.05	0.38	0.59	0.51	0.47	0.58
0°: minimum negative values	−1.46	−0.81	−1.66	−2.15	−1.20	−1.54	−0.51
90°: minimum negative values	−1.53	−1.26	−1.58	−1.36	−1.64	−0.94	−0.77

According to the above two tables, the displacement mean value diagram and displacement variation range diagram of each monitoring point at the 0° and 90° wind direction angles in the wind tunnel test can be made, as shown in Figure 13.

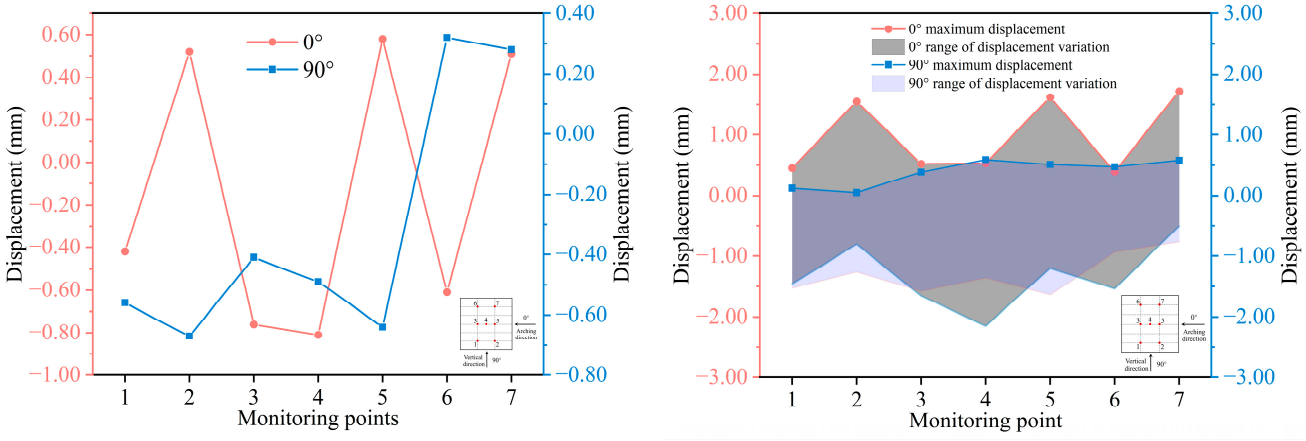

(**a**) Mean displacement (**b**) Range of displacement variation

Figure 13. Displacement diagram of each monitoring point under a wind tunnel test.

It can be seen from Figure 13a that the average displacements of points 2, 5 and 7 are greater than 0 at the 0° wind direction angle, which means that the three monitoring points produce the overall downward displacement vibration. The average displacement of the remaining monitoring points is less than 0, which means that each monitoring point generates an overall upward displacement vibration. At the wind direction angle of 90°, the average displacements of points 6 and 7 are greater than 0; that is, the overall downward displacement vibration is generated. The average displacement of the remaining monitoring points is less than 0, which means that each monitoring point generates an overall upward displacement vibration.

It can be seen from Figure 13b that the maximum displacement of each monitoring point changes greatly under the action of the 0° wind direction angle, and the maximum displacement of each monitoring point changes smoothly under the 90° wind direction angle. Comparing the variation range of 0° and 90° wind direction angle displacement, it can be seen that the vibration amplitude of different regions of the saddle membrane structure is quite different under the 0° wind direction angle. Especially in the large membrane structure of practical engineering, this difference will be more significant, so we should be more vigilant about the influence of the flow in this direction on the membrane structure.

3. Numerical Simulations

3.1. Numerical Simulation Process

3.1.1. Simulation Condition Setting

The wind-induced vibration response of membrane structures involves geometric nonlinearity and fluid–solid coupling calculation. In the ANSYS finite element software, the Mechanical module can solve the geometric nonlinearity, and the FLUENT module can solve the fluid dynamics problem. The calculation data of different modules are transmitted through the System Coupling module, so the ANSYS finite element software can solve the wind vibration response of the membrane structure. Large eddy simulation is selected as the turbulence model. Large eddy simulation refers to the establishment of models for small-scale turbulence pulsations, which can obtain richer turbulence information. If the turbulence model is too simplified, only the average information of turbulence can be obtained, which will affect the subsequent fluid–solid coupling calculation accuracy. It is proposed to use the working conditions consistent with the test model for finite element simulation, and the specific working conditions are shown in Table 4.

Table 4. Numerical simulation condition table.

Working Condition	Simulation Model Size	Turbulent Flow Model	Wind Direction Angle	Wind Field
1	Consistent with the size of the test model	Large eddy simulation	0°	Equation (1)
2			90°	Equation (2)

3.1.2. Fluid Domain and Grid Division Settings

The fluid computational region and model size for numerical simulations are consistent with the test dimensions. The size of the fluid domain in the downstream, vertical and spreading directions are 25.0 m, 3.6 m and 6.0 m, respectively, and the arch span length, vertical span length and rise–span ratio of the model are 1 m, 1 m and 1/8, respectively. In order to reduce the waste of computing resources caused by grid update and reconstruction in fluid–solid coupling calculation, the basin is divided into blocks. The basin containing the membrane structure involves the update and reconstruction of the grid. This part adopts tetrahedral grid division, and the grid near the junction of the membrane and the flow field is properly encrypted, and the rest of the basin is divided by the hexahedral grid. ICEM software is used to divide the basin into grids, and the total number of grids is about 650,000. The basin size and grid division are shown in Figure 14, and the specific grid division parameters are shown in Table 5.

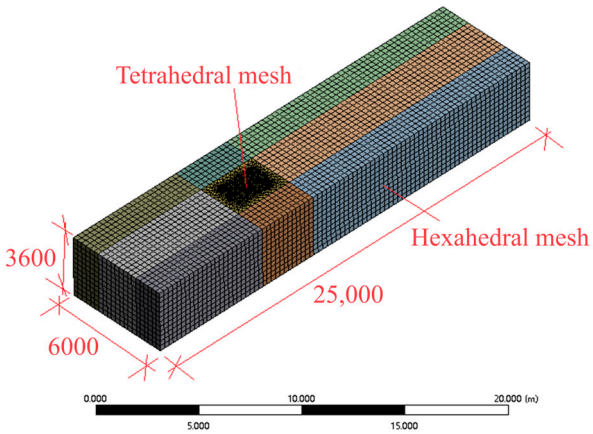

Figure 14. Watershed and grid division.

Table 5. Meshing parameters.

Type	Grid Control Parameters	Parameter Value
Grid reconstruction area	Mesh type	Unstructured tetrahedral grid
	Maximum unit size	Basin: 0.25 m
		Membrane: 0.05 m
	Near-wall grid	Thickness of the first layer unit: 0.05 m Growth rate: 1.2 Expansion number of layers: 15
General area	Mesh type	Structured hexahedral mesh
	Maximum unit size	Basin: 0.25 m
	Near-wall grid	Thickness of the first layer unit: 0.08 m Growth rate: 1.2 Expansion number of layers: 8

3.1.3. Boundary Condition Setting

In the fluid domain calculation simulation, the velocity inlet boundary condition and the pressure outlet boundary condition are used. Equations (1) and (2) are compiled into

the velocity inlet boundary conditions of FLUENT by UDF programming, and the Vortex method is used to generate turbulent pulsation at the inlet boundary. The top and side of the flow field are set as the symmetrical boundary of the free slip wall, and the lower surface is set as a non-slip wall boundary condition. The tetrahedral mesh region is updated and reconstructed by remeshing technology and diffusion smoothing technology, and the interface between the membrane structure and the flow field is defined as the fluid–solid coupling surface. For the structural module, the membrane is discretized by the SHELL181 element, and the boundary conditions are set to be consistent with the boundary conditions in the test model, that is, the four-sided fixed support boundary conditions. The flow field and structural boundary settings are shown in Figure 15, and the specific parameter settings of FLUENT are shown in Table 6.

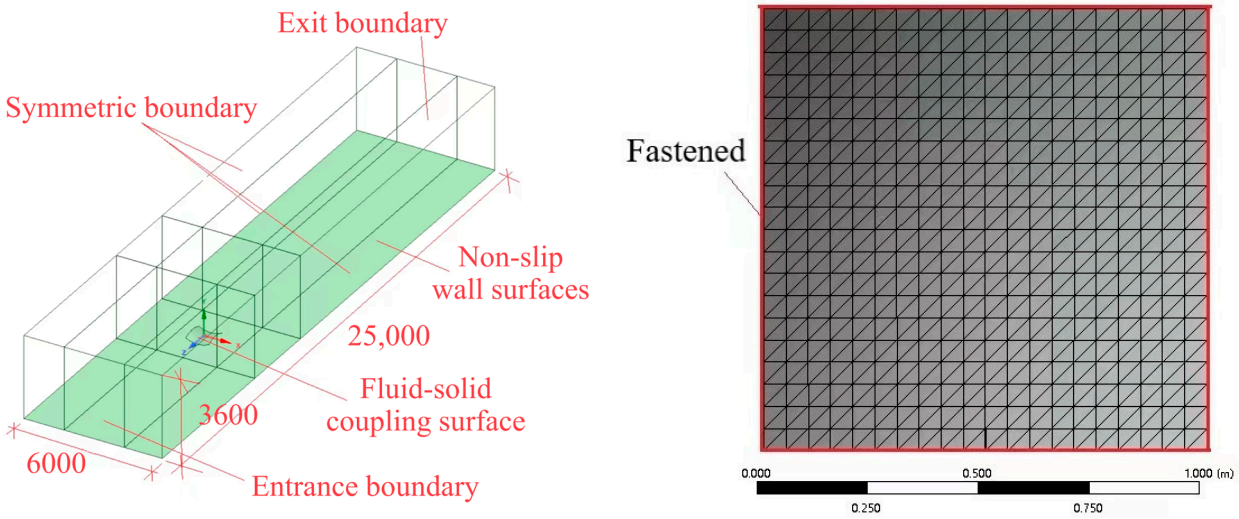

(**a**) Flow field (**b**) Boundary

Figure 15. Boundary condition setting.

Table 6. Basic parameters and boundary conditions.

Type	Parameter Setting
Type of solver	Pressure-based transient solution
Turbulent flow model	Large eddy simulation
Inflow boundary condition	Vortex method generates turbulent pulsation
Outlet boundary condition	Pressure outlet
Wall boundary condition	Non-slip wall
Dynamic grid settings	Diffusion smoothing; mesh rezoning
Numerical solution algorithm	SIMPLE
Convection term solution format	Second-order upwind scheme
Convergence residual standard	10^{-3}

3.1.4. Fluid-Solid Coupling Parameter Setting

Data transmission in fluid–solid coupling refers to the exchange and transmission of fluid and solid calculation results through the fluid–solid interface. Mapping and interpolation calculation are indispensable links to complete data exchange. In ANSYS, System Coupling is the main module to control the iterative parameters of fluid–solid coupling and interface data exchange settings, and its combination analysis process is shown in Figure 16.

In the System Coupling module, the solution order of the flow field is set to 1, and the solution order of the structure is set to 2. Under this setting, the system first solves the flow field, then the pressure of the flow field is mapped to the solid surface to cause solid deformation, and finally the solid deformation causes the flow field to change, and the

solution is solved in this iterative order. The fluid–solid coupling iteration frequency in the simulation is set to be consistent with the data acquisition frequency in the wind tunnel test, both of which are 0.005 s. The total calculation time is set to 30 s, and the result output frequency is selected as All Step for subsequent data analysis.

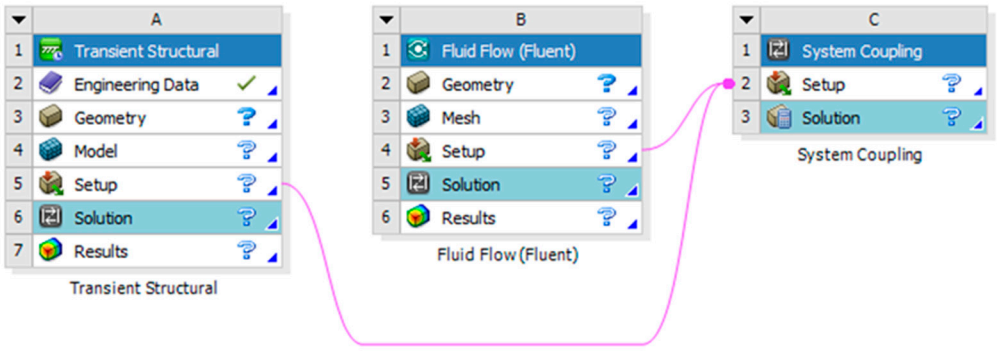

Figure 16. Fluid–solid coupling module in Workbench.

3.2. Simulation Result Analysis

Figure 17 presents the flow velocity profile and wind pressure distribution near the structure at a certain moment in the steady-state vibration stage under the wind direction angles of 0° and 90°. When the wind blows to the membrane structure along the 0° wind direction angle, the wind field is divided into two parts at the leading edge of the structure. The wind speed of the upper flow field is larger, the wind direction changes along the curvature of the membrane and the wind speed of the leeward side of the flow field is larger than that of the windward side. The lower flow field is less disturbed by the incoming flow and the flow velocity is slower. At this time, the windward side and the center of the membrane are negative wind pressure, and the leeward side is positive wind pressure, and the farther away from the front of the structure, the greater the wind pressure. When the wind blows to the membrane structure along the 90° wind direction angle, the flow velocity on the membrane is opposite to the 0° direction angle. At this time, most of the windward surface is negative wind pressure, and the rest of the membrane is positive wind pressure distribution, and the farther away from the front of the structure, the greater the wind pressure.

As discussed in the wind tunnel test section, the amount of data collected by the numerical simulation is large. At the same time, in order to compare and analyze the wind tunnel test and numerical simulation, the displacement response curves of monitoring points 2 and 4 at 0° and 90° wind direction angles are given, as shown in Figure 18. The displacement responses of the remaining points only show the mean and extreme values (maximum positive values and minimum negative values). Compared with the data of the wind tunnel test, the data of numerical simulation have great volatility and strong disorder. One of the reasons for this phenomenon is that fluid–solid coupling involves the updating and reconstruction of element grids, which will inevitably make the quality of grids uneven and affect the calculation accuracy. In addition, another reason is that in the fluid–solid coupling calculation, the data mapping between the structural solver and the fluid solver is not convergent, resulting in a large fluctuation of the calculation results.

Similarly, in order to obtain accurate statistical data as much as possible and reduce the randomness and uncertainty in the numerical simulation process, the displacement mean and displacement extreme value of 30 s in the steady-state stage are calculated. Table 7 shows the average displacement of each monitoring point at 0° and 90° wind direction angles in numerical simulation. Table 8 shows the displacement extreme values of each monitoring point under 0° and 90° wind direction angles in numerical simulation.

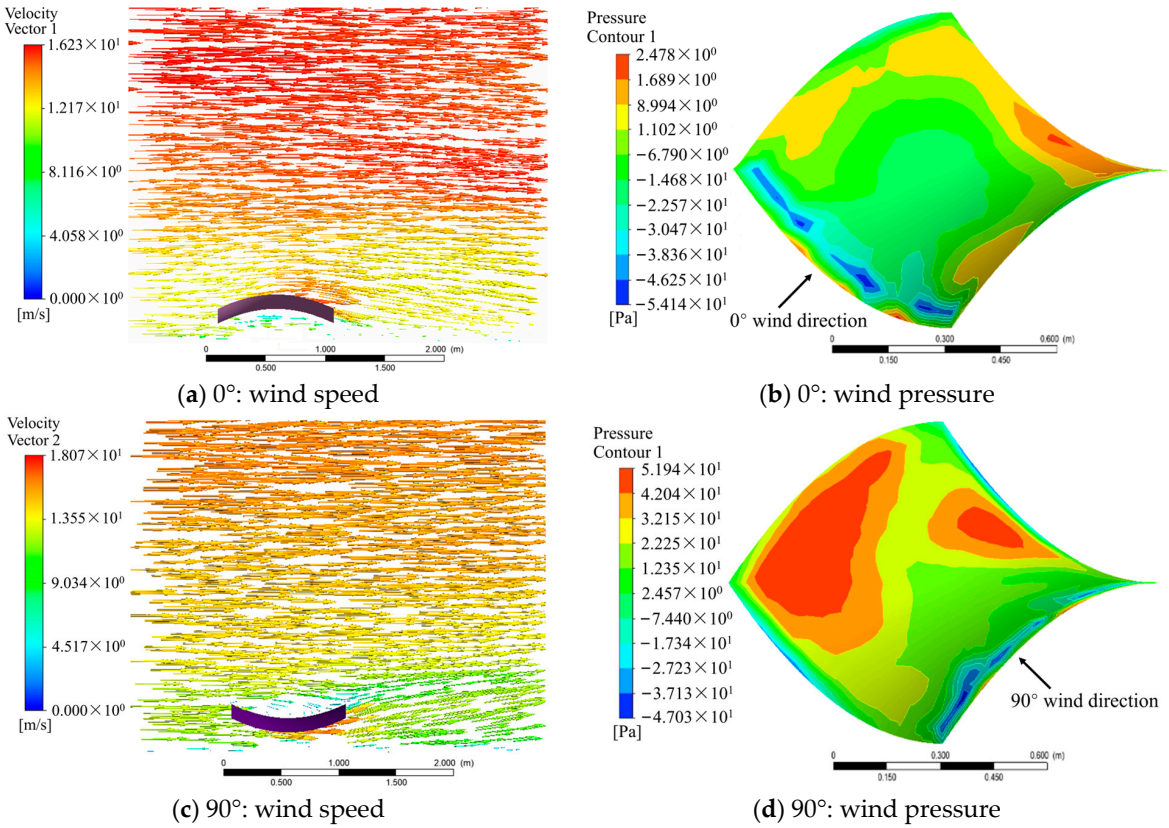

(**a**) 0°: wind speed (**b**) 0°: wind pressure

(**c**) 90°: wind speed (**d**) 90°: wind pressure

Figure 17. Distribution of wind speed and wind pressure in steady-state vibration stage.

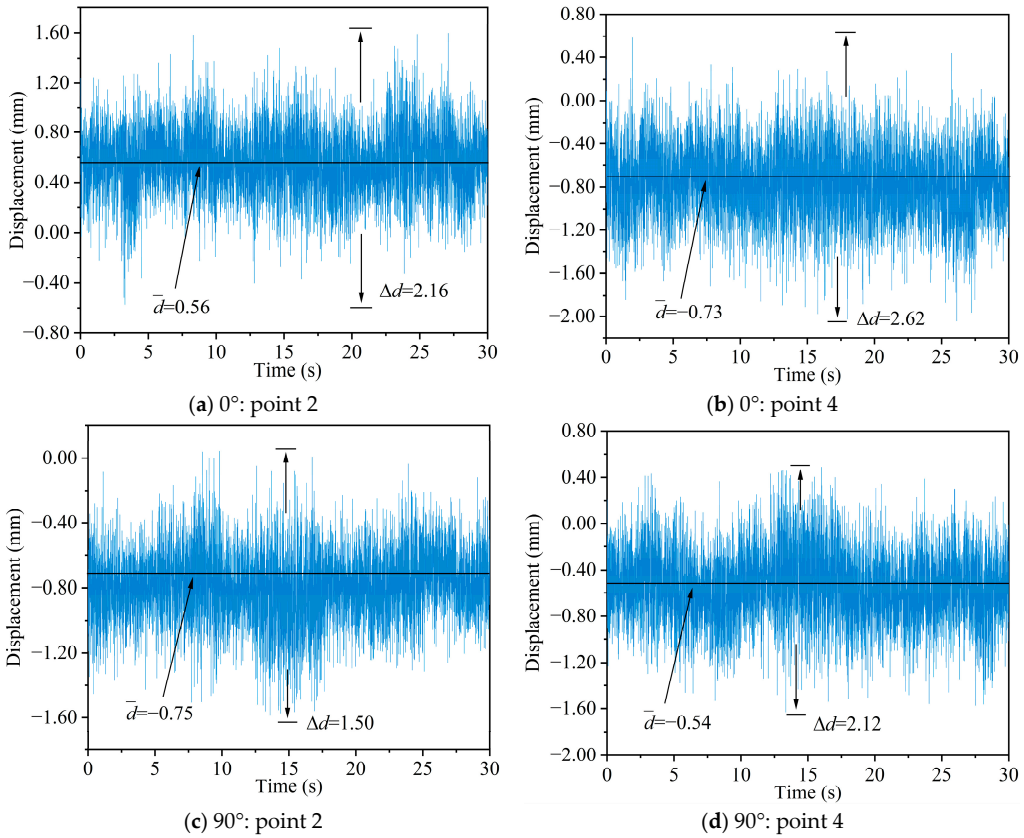

(**a**) 0°: point 2 (**b**) 0°: point 4

(**c**) 90°: point 2 (**d**) 90°: point 4

Figure 18. Displacement response curve under numerical simulation.

Table 7. Mean values of displacement at each point under numerical simulation (mm).

Wind Direction Angle: Displacement	Point 1	Point 2	Point 3	Point 4	Point 5	Point 6	Point 7
0°	−0.47	0.56	−0.66	−0.73	0.51	−0.54	0.46
90°	−0.61	−0.75	−0.46	−0.54	−0.69	0.35	0.31

Table 8. Displacement extremes at each point under numerical simulation (mm).

Wind Direction Angle: Displacement	Point 1	Point 2	Point 3	Point 4	Point 5	Point 6	Point 7
0°: maximum positive values	0.58	1.57	0.31	0.61	1.45	0.22	1.15
90°: maximum positive values	0.31	−0.08	0.61	0.49	0.64	0.53	0.64
0°: minimum negative values	−1.14	−0.59	−1.65	−2.01	−0.94	−1.50	−1.31
90°: minimum negative values	−1.50	−1.58	−1.59	−1.63	−1.67	−1.02	−0.76

According to Tables 7 and 8, the mean displacement and displacement range of each monitoring point in the numerical simulation can be made, as shown in Figure 19. Comparing Figure 13, it can be seen that the mean value of displacement and the trend of displacement change in the numerical simulation are not much different from those in the wind tunnel test. This phenomenon also proves that the fluid–solid coupling numerical calculation results of the membrane structure have high reliability and are more in line with the actual engineering situation.

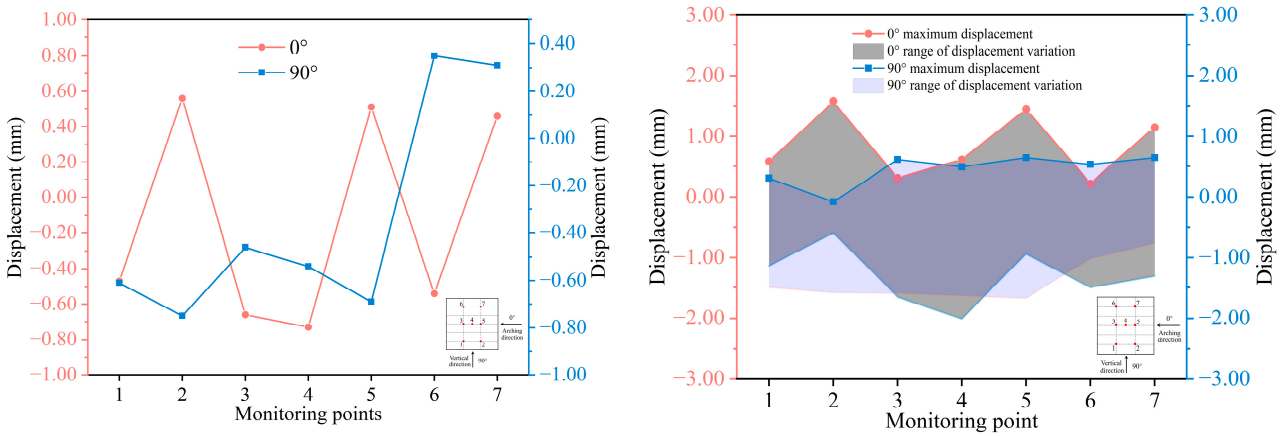

(**a**) Mean displacement (**b**) Range of displacement variation

Figure 19. Displacement diagram of each monitoring point under numerical simulation.

4. Comparison of Wind Tunnel Test and Numerical Simulation Results

In order to explore the errors between the wind tunnel test and numerical simulation, this section first analyzes the absolute error and relative error, and then it analyzes the curve shape of the two from the perspectives of probability density, skewness and kurtosis, and points out the problems existing in the wind tunnel test and numerical simulation, so as to facilitate the optimization of subsequent research.

4.1. Absolute Error of Mean and Range

In order to quantitatively compare the results of the wind tunnel test and numerical simulation, the calculation formula of absolute error is defined as follows:

$$\Delta_{ae} = |d_t - d_s| \tag{4}$$

d_t represents the mean displacement of a monitoring point under a certain wind direction angle in the wind tunnel test. d_s represents the mean displacement of a monitoring

point under a certain wind direction angle in numerical simulation. Therefore, according to Tables 2 and 7, the absolute error of the mean displacement of each monitoring point in the wind tunnel test and numerical simulation can be calculated, as shown in Table 9.

Table 9. Absolute error of mean displacement between wind tunnel test and numerical simulation (mm).

Wind Direction Angle	Point 1	Point 2	Point 3	Point 4	Point 5	Point 6	Point 7	Average of Each Point
0°	0.05	0.04	0.10	0.08	0.07	0.07	0.05	0.07
90°	0.05	0.08	0.05	0.05	0.05	0.03	0.03	0.05

Tables 3 and 8 give the maximum positive values and minimum negative values of displacement under the wind tunnel test or numerical simulation. In order to evaluate the error between the two methods by using these two extreme values, and taking into account the degree of dispersion of the data, the range is introduced for analysis. The formula of the range is as follows:

$$r = \Delta d = d_{\max} - d_{\min} \tag{5}$$

By introducing Equations (4) and (5) to the presented results in Tables 3 and 8, the absolute error of the displacement range can be readily obtained, as given in Table 10.

Table 10. Absolute error of displacement range between wind tunnel test and numerical simulation (mm).

Wind Direction Angle	Point 1	Point 2	Point 3	Point 4	Point 5	Point 6	Point 7	Average of Each Point
0°	0.19	0.20	0.22	0.06	0.43	0.21	0.23	0.22
90°	0.16	0.19	0.24	0.17	0.16	0.14	0.05	0.16

To further vividly observe the pattern of absolute error more, the presented results in Tables 9 and 10 have been depicted in a graph as illustrated in Figure 20.

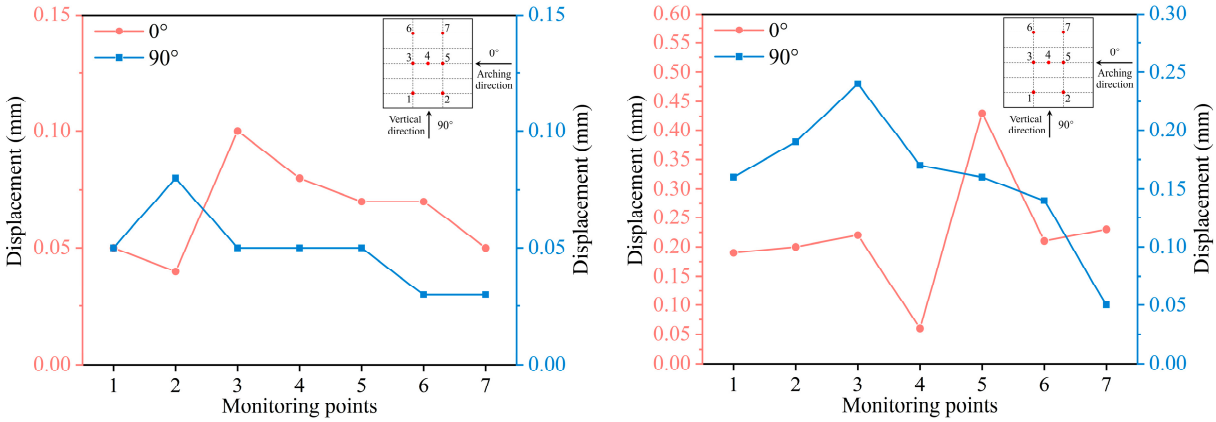

(**a**) Mean displacement (**b**) Displacement range

Figure 20. Absolute error of each monitoring point.

It can be seen from Figure 20a that the absolute error of the mean displacement of the wind tunnel test and numerical simulation under different direction angles and different monitoring points is less than 0.10 mm. It can be seen from Figure 20b that the absolute error of the displacement range of the wind tunnel test and numerical simulation at different direction angles and different monitoring points is less than 0.45 mm. Because the range is the relationship between the maximum positive values and the minimum negative values, which reflects the range of displacement response, the results are within the acceptable range.

At the same time, focusing on the common trend of the two subgraph curves, it can be seen that there are obvious peaks at points 3, 4 and 5, which also correspond to the central area of the membrane. The central area of the membrane is less constrained, and the wind-induced response under the action of wind load is more complex. Therefore, the error obtained by the two methods is larger here. Subsequently, more monitoring points can be arranged in the central area of the membrane to collect as much data as possible to take the average value and reduce the occurrence of errors.

4.2. Relative Error of Mean and Range

At the same time, in order to further understand the degree of change in the displacement difference relative to the test value and the simulated value, the calculation formula of the relative error is defined as follows:

$$\Delta_{re} = \frac{|d_t - d_s|}{|d_t|} \times 100\% \quad (6)$$

According to the above formula, the relative error of displacement mean and displacement range between the wind tunnel test and numerical simulation at each point can be calculated. The results are shown in Tables 11 and 12.

Table 11. Relative error of mean displacement between wind tunnel test and numerical simulation (%).

Wind Direction Angle	Point 1	Point 2	Point 3	Point 4	Point 5	Point 6	Point 7	Average of Each Point
0°	11.90	7.69	13.16	9.88	12.07	11.48	9.80	10.85
90°	8.93	11.94	12.20	10.20	7.81	9.37	10.71	10.17

Table 12. Relative error of displacement range between wind tunnel test and numerical simulation (%).

Wind Direction Angle	Point 1	Point 2	Point 3	Point 4	Point 5	Point 6	Point 7	Average of Each Point
0°	9.95	8.47	10.09	2.24	15.25	10.88	10.31	9.60
90°	9.70	14.50	12.24	8.72	7.44	9.93	3.70	9.46

To further vividly observe the pattern of relative error more, the presented results in Tables 11 and 12 have been depicted in a graph as illustrated in Figure 21.

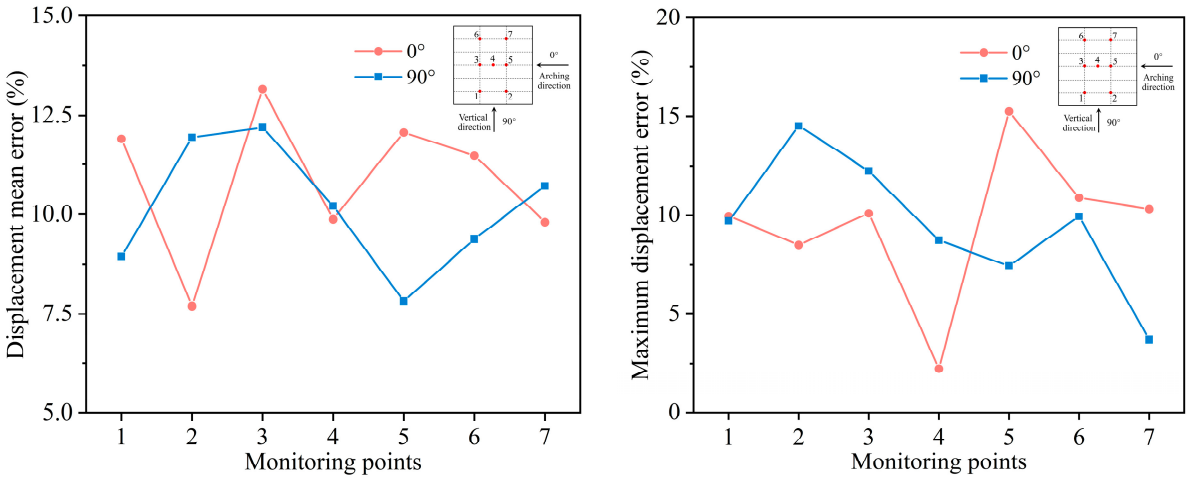

(**a**) Mean displacement (**b**) Displacement range

Figure 21. The relative error of each monitoring point.

From Figure 21a, it can be seen that the relative error of the mean displacement of point 3 is the largest at the 0° wind direction angle, and the error reaches 13.16%. When

the wind direction angle is 90°, the relative error of the mean displacement of point 3 also reaches the maximum, and the error reaches 12.20%. The average relative error between the test and the simulated displacement mean value of each monitoring point is about 10.85%. The relative error of the displacement mean value of all monitoring points is less than 15%. This phenomenon proves that the overall reduction degree of the numerical simulation results is good.

From Figure 21b, it can be seen that the maximum relative error of the displacement range occurs at point 5 at the 0° wind direction angle, and the error reaches 15.25%. When the wind direction angle is 90°, the maximum relative error of the displacement range occurs at point 2, and the error reaches 14.50%. The average relative error between the test and the simulated displacement range for each monitoring point is less than 10%, while the maximum relative error for all monitoring points is less than 20%. This reveals that the simulation model has a strong capability to capture the maximum amplitude of the wind-induced vibration response of the membrane structure.

4.3. Skewness and Kurtosis

Due to the large amount of data on vibration response, it is difficult to intuitively analyze the difference between the test results and the simulation results only by means of statistics such as mean value and range. Therefore, the capture ability of numerical simulation to real results is discussed from the perspective of probability density. Figure 22 presents the displacement statistical curve of monitoring points 2 and 4 at the 0° wind direction angle. Each point in the diagram represents the probability of corresponding displacement, and the curve is the result of Gaussian fitting of the actual displacement value. It can be seen from this set of figures that the coincidence degree of the probability density curve between the test and the simulation is high, indicating that the statistical results of the vibration response of the numerical simulation are less different from the test.

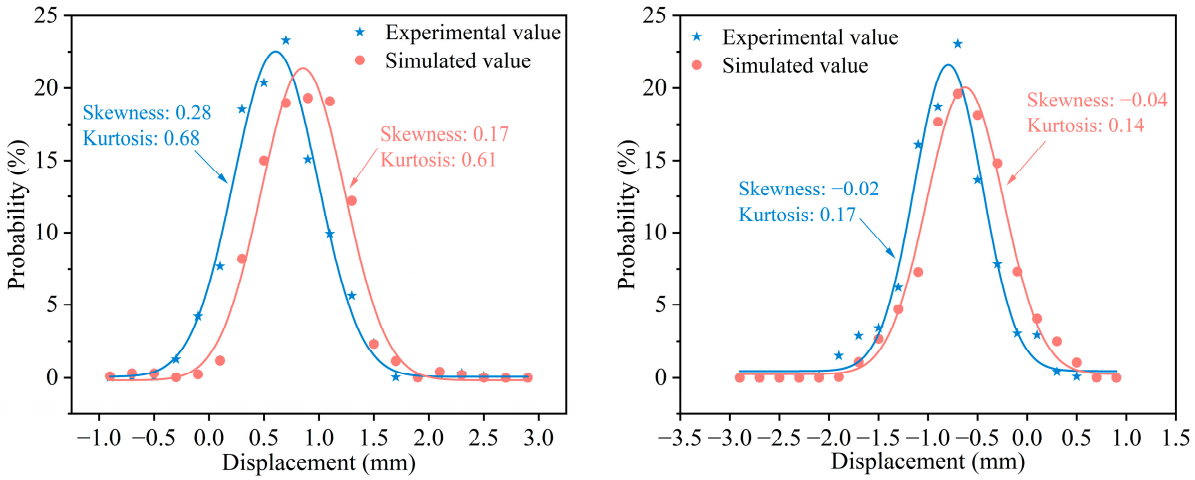

(**a**) Point 2 (**b**) Point 4

Figure 22. The probability density curves of points 2 and 4 under 0° wind direction angle.

At the same time, skewness and kurtosis are introduced to study the distribution of data. Both skewness and kurtosis are the characteristic numbers describing the distribution shape of the curve. The skewness, also known as the skewness coefficient, is defined as follows:

$$Sk(X) = E[(\frac{X-\mu}{\sigma})^3] \quad (7)$$

where μ is the mean value and σ is the standard deviation. Skewness is a measure of the skew direction and degree of statistical data distribution, and it is a digital feature of the asymmetry degree of statistical data distribution. For the normal distribution, the skewness

is 0, and the tail lengths on both sides are symmetrical. If the skewness of the distribution is less than 0, it indicates that the distribution has a negative deviation, that is, the left skewness. At this time, the data on the left side of the mean are less than that on the right side. The tail on the left side is longer than that on the right side, because there are a few variables with very small values, which makes the tail on the left side of the curve drag very long. If the skewness of the distribution is greater than 0, it is right skewed. At this time, the data on the right side of the mean are less than that on the left side, and the tail on the right side is longer than that on the left side. Because there are a few variables with large values, the tail on the right side of the curve is dragged very long.

Observing the shape and distribution of the curve, whether it is the probability density curve of the test or simulation, the probability density curve of the vibration response of point 2 has a certain left bias, and point 4 has a certain right bias. This shows that the wind-induced vibration of the membrane does not obey the Gaussian distribution but has a certain bias, which is determined by the unsteady nature of the wind field and the geometric nonlinearity of the structural vibration.

Kurtosis, also known as the kurtosis coefficient, is defined as follows:

$$Ku(X) = E[(\frac{X-\mu}{\sigma})^4] - 3 \quad (8)$$

Kurtosis is a characteristic number that characterizes the peak value of the probability density curve at the average value, which can be used to measure the outlier of the data. Kurtosis is a measurement of the flat peak or peak degree of data distribution. Intuitively, kurtosis reflects the sharpness of the peak of the wind-induced displacement response curve. When the kurtosis coefficient is greater than 0, the distribution of data is more concentrated. When the kurtosis coefficient is less than 0, the distribution of the data is more dispersed. Comparing the kurtosis of the probability density curves of the two monitoring points, it is found that the kurtosis of the simulation results is smaller than that of the test, indicating that the dispersion degree of the simulation results is larger than that of the test results.

5. Conclusions

The dynamic response of the saddle membrane structure under the action of wind load is studied by wind tunnel tests and numerical simulations. The novel aspect is to introduce parameters such as statistics to compare and analyze the results obtained by tests and simulations. The following conclusions are obtained:

1. The maximum displacement of each monitoring point at the 0° wind direction angle (arching direction) changes greatly, and the maximum displacement of each monitoring point at the 90° wind direction angle (vertical direction) changes more smoothly. Therefore, it is necessary to be alert to the influence of the 0° wind direction angle (arching direction) on the membrane structure. When the actual engineering structure is arranged, the arching direction of the saddle membrane structure can be along the main direction of the local wind. Furthermore, the wind-induced vibration displacement of the membrane structure is reduced at the design level.
2. Both wind tunnel tests and numerical simulations are the main methods to study the wind-induced vibration of membrane structures. The absolute errors of the mean displacement and the displacement range obtained by the two methods are less than 0.10 mm and 0.45 mm, respectively, and the relative errors of the mean displacement and the displacement range are about 10%. Therefore, it can be explained that the data obtained from the wind tunnel test and numerical simulation are reliable, which is conducive to the introduction of statistical parameters for analysis.
3. The central area of the membrane is less constrained, and the wind-induced response under the action of wind load is more complicated. Therefore, the error obtained by the two methods here is large. Subsequently, more monitoring points can be arranged in the central area of the membrane to collect as much data as possible to take the average value and reduce the occurrence of errors. In actual engineering structures,

the displacement response is greater in the center of the membrane. A reinforcing material can be added to the center area, or a thicker membrane can be used overall.

4. Comparing the displacement response probability density curve fitted by wind tunnel tests and numerical simulations, it can be found that the two have a good coincidence degree. However, it can be seen from the skewness data that both of them show a certain skewed distribution, indicating that the wind-induced vibration displacement of the membrane does not obey the Gaussian distribution. If the performance function established by displacement as a variable does not conform to the normal distribution in the subsequent study of membrane structure reliability, it is necessary to select an appropriate method to solve it, such as the 'equivalent normalization' method. At the same time, by analyzing the kurtosis parameters, it can be seen that the results obtained by the wind tunnel test have good stability, while the displacement response of numerical simulation is more discrete. If the numerical simulation method is continued, the number of computational grids can be increased and more accurate results can be obtained. For the actual engineering structure, the structure size is larger and more complex, and the numerical simulation parameter setting can provide a reference. However, the number of computational grids should be further increased to achieve higher accuracy.

Author Contributions: Conceptualization, J.L. and X.D.; Data curation, Z.C.; Formal analysis, Z.C. and C.L. (Changjiang Liu); Investigation, J.L., X.D. and C.L. (Chiyu Luo); Methodology, D.L.; Project administration, C.L. (Changjiang Liu) and D.L.; Resources, C.L. (Chiyu Luo) and G.Z.; Software, Z.C.; Validation, D.L. and G.Z.; Writing—original draft, Z.C.; Writing—review and editing, C.L. (Changjiang Liu). All authors will be informed about each step of manuscript processing including submission, revision, revision reminder, etc. via emails from our system or assigned Assistant Editor. All authors have read and agreed to the published version of the manuscript.

Funding: This research was funded by the National Natural Science Foundation of China (Project Number 52108121), Guangdong Basic and Applied Basic Research Foundation (Project Number 2019A1515011063), Guangzhou Science and Technology Project (Project number 202102010455).

Data Availability Statement: The original contributions presented in the study are included in the article, further inquiries can be directed to the corresponding authors.

Conflicts of Interest: Author Guangen Zhou was employed by the company Zhejiang Southeast Space Frame Co., Ltd. The remaining authors declare that the research was conducted in the absence of any commercial or financial relationships that could be construed as a potential conflict of interest.

References

1. De Smedt, E.; Mollaert, M.; Caspeele, R.; Botte, W.; Pyl, L. Reliability-based calibration of partial factors for the design of membrane structures. *Eng. Struct.* **2020**, *214*, 110632. [CrossRef]
2. Zhang, L.; Zhang, Y.; Song, W.; Xu, J.; Xue, J. A nonlinear damage constitutive model of PVC coated fabrics. *Structures* **2021**, *30*, 368–377. [CrossRef]
3. Ying, J.; Huang, J.; Qin, S.; Huang, Y. On the Mechanical and Electrical Properties of the Composite Structure of PVC Membrane and Thin-Film Battery under Biaxial Tension. *Appl. Sci.* **2021**, *11*, 6830. [CrossRef]
4. Zhang, Y.; Lu, Y.; Zhou, Y.; Zhang, Q. Resistance uncertainty and structural reliability of hypar tensioned membrane structures with PVC coated polyesters. *Thin-Walled Struct.* **2018**, *124*, 392–401. [CrossRef]
5. Liu, C.; Xie, H.; Deng, X.; Liu, J.; Wang, M.; Jiang, S. Random vibration of composite saddle membrane structure under the impact loading. *Compos. Struct.* **2021**, *269*, 114020. [CrossRef]
6. Liu, C.; Deng, X.; Liu, J.; Peng, T.; Yang, S.; Zheng, Z. Dynamic response of saddle membrane structure under hail impact. *Eng. Struct.* **2020**, *214*, 110597. [CrossRef]
7. Liu, C.; Wang, M.; Deng, X.; Li, D.; Liu, J.; Wang, X. Impact of saddle membrane structure by hail with combined particle sizes: Numerical simulation and experimental investigation. *Eng. Struct.* **2022**, *264*, 114477. [CrossRef]
8. Zheng, Z.; Zhang, G.; Li, D.; Liu, C. Dynamic response of rectangular membrane excited by heavy rainfall. *J. Vib. Control.* **2019**, *25*, 777–792. [CrossRef]
9. Sun, X.Y.; He, R.J.; Wu, Y. Numerical simulation of snowdrift on a membrane roof and the mechanical performance under snow loads. *Cold Reg. Sci. Technol.* **2018**, *150*, 15–24. [CrossRef]

10. Cui, W.; Zhao, L.; Ge, Y.J. Wind-Induced Buffeting Vibration of Long-Span Bridge Considering Geometric and Aerodynamic Nonlinearity Based on Reduced-Order Modeling. *J. Struct. Eng.* **2023**, *149*, 04023160. [CrossRef]
11. Cui, W.; Caracoglia, L.; Zhao, L.; Ge, Y.J. Examination of occurrence probability of vortex-induced vibration of long-span bridge decks by Fokker-Planck-Kolmogorov equation. *Struct. Saf.* **2023**, *105*, 102369. [CrossRef]
12. Jacome, L.B.; Elham, A. Wing Aerostructural Optimization under Uncertain Aircraft Range and Payload Weight. *J. Aircr.* **2017**, *54*, 1109–1120. [CrossRef]
13. Maraveas, C.; Tsavdaridis, K.D. Assessment and retrofitting of an existing steel structure subjected to wind-induced failure analysis. *J. Build. Eng.* **2019**, *23*, 53–67. [CrossRef]
14. Gu, M. Wind-resistant studies on tall buildings and structures. *Sci. China-Technol. Sci.* **2010**, *53*, 2630–2646. [CrossRef]
15. Tamura, Y.; Kim, Y.C.; Kikuchi, H.; Hibi, K. Correlation and combination of wind force components and responses. *J. Wind. Eng. Ind. Aerodyn.* **2014**, *125*, 81–93. [CrossRef]
16. Ke, S.; Wang, H.; Ge, Y. Wind load effects and equivalent static wind loads of three-tower connected tall buildings based on wind tunnel tests. *Struct. Eng. Mech.* **2016**, *58*, 967–988. [CrossRef]
17. Li, Z.; Wang, D.; Chen, X.; Liang, S.; Li, J. Wind load effect of single-column-supported two-plate billboard structures. *J. Wind. Eng. Ind. Aerodyn.* **2018**, *179*, 70–79. [CrossRef]
18. Daniels, S.J.; Xie, Z. Overview of large-eddy simulation for wind loading on slender structures. *Proc. Inst. Civ. Eng. -Eng. Comput. Mech.* **2022**, *175*, 41–71. [CrossRef]
19. Luo, N.; Jia, H.; Liao, H. Coupled wind-induced responses and equivalent static wind loads on long-span roof structures with the consistent load-response-correlation method. *Adv. Struct. Eng.* **2018**, *21*, 71–81. [CrossRef]
20. Huang, P.; Zhou, X.-Y.; Gu, M. Experimental study of wind loads on cylindrical reticulated shells. *Appl. Math. Mech. -Engl. Ed.* **2013**, *34*, 281–296. [CrossRef]
21. Wang, Y.X.; Xu, J.K.; Qiao, L.; Zhang, Y.; Bai, J.Q. Improved Amplification Factor Transport Transition Model for Transonic Boundary Layers. *AIAA J.* **2023**, *61*, 3866–3882. [CrossRef]
22. Cui, W.; Zhao, L.; Ge, Y.J.; Xu, K. A generalized van der Pol nonlinear model of vortex-induced vibrations of bridge decks with multistability. *Nonlinear Dyn.* **2024**, *112*, 259–272. [CrossRef]
23. Wang, Y.; Gong, J.; Liu, Y.; Shi, C.; Zheng, J. Effect of climate change on flexural reliability of highway continuous girder bridge under wind load. *Bridge Struct.* **2019**, *15*, 103–110. [CrossRef]
24. Xu, J.; Zhang, Y.; Wu, M.; Li, X.; Zhang, L. Damping characteristics of the architectural coated fabric and its influence on the vibration response of membrane structures. *Compos. Struct.* **2022**, *285*, 115207. [CrossRef]
25. Li, D.; Zheng, Z.; Liu, C.; Zhang, G.; Lian, Y.; Tian, Y.; Xiao, Y.; Xie, X. Dynamic response of rectangular prestressed membrane subjected to uniform impact load. *Arch. Civ. Mech. Eng.* **2017**, *17*, 586–598. [CrossRef]
26. Kandel, A.; Sun, X.Y.; Wu, Y. Wind-induced responses and equivalent static design method of oval-shaped arch-supported membrane structure. *J. Wind. Eng. Ind. Aerodyn.* **2021**, *213*, 104620. [CrossRef]
27. Wang, Z.; Zhang, Y.; Qin, Z. Response prediction and fatigue life estimation of thin-walled structures under random excitation using the modified equivalent linearization method. *Thin-Walled Struct.* **2023**, *188*, 110824. [CrossRef]
28. Chen, Z.Q.; Wei, C.; Yin, L.; Su, N.; Zhao, J.B.; Wu, Y. Interference effects on the wind loads and wind-induced responses of parallel-arranged rectangular-planed air-supported membrane structures. *Thin-Walled Struct.* **2024**, *197*, 111572. [CrossRef]
29. He, Y.L.; Zhu, M.X.; Zhao, Y.G.; Li, X.Y. Influence of different cable-membrane connection models on wind-induced responses of an air supported membrane structure with orthogonal cable net. *Thin-Walled Struct.* **2022**, *180*, 109840. [CrossRef]
30. Zhang, X.L.; Ju, Y.Z.; Wang, F.W. Statistical Analysis of Wind-Induced Dynamic Response of Power Towers and Four-Circuit Transmission Tower-Line System. *Shock. Vib.* **2018**, *2018*, 5064930. [CrossRef]
31. Chen, Z.; Yin, L.; Tang, L.; Wang, S. Aero-elastic behavior of open-type one-way tensioned membrane structure models. *AIP Adv.* **2021**, *11*, 105201. [CrossRef]
32. Wood, J.N.; Breuer, M.; De Nayer, G. Experimental studies on the instantaneous fluid-structure interaction of an air-inflated flexible membrane in turbulent flow. *J. Fluids Struct.* **2018**, *80*, 405–440. [CrossRef]
33. Chen, Z.Q.; Wei, C.; Chen, Z.Z.; Wang, S.; Tang, L.X. Numerical Simulation of Atmospheric Boundary Layer Turbulence in a Wind Tunnel Based on a Hybrid Method. *Atmosphere* **2022**, *13*, 2044. [CrossRef]
34. Michalski, A.; Gawenat, B.; Gelenne, P.; Haug, E. Computational wind engineering of large umbrella structures. *J. Wind. Eng. Ind. Aerodyn.* **2015**, *144*, 96–107. [CrossRef]
35. Michalski, A.; Haug, E.; Wuechner, R.; Bletzinger, K.U. Validation of a virtual design methodology for the structural analysis of membrane structures subjected to wind. *Bauingenieur* **2011**, *86*, 129–141.
36. Kawulok, M.; Freiherrova, N.; Hornakova, M.; Juracka, D.; Krejsa, M. Hyperbolic Paraboloid Tensile Structure-Numerical CFD Simulation of Wind Flow in RWIND Software. *Buildings* **2023**, *13*, 681. [CrossRef]
37. Sun, F.J.; Tang, H.X.; Lu, M.J.; Zhang, D.M.; Lu, C. A Study on Wind Pressure Characteristics of a Large-Span Membrane Structure under the Fluctuating Wind in a Vertical Direction Based on a Large Eddy Simulation. *Model. Simul. Eng.* **2022**, *2022*, 8209487. [CrossRef]
38. Xu, J.; Zhang, Y.; Zhang, L.; Wu, M.; Zhou, Y.; Lei, K.; Zhang, Q. Wind-induced response of open type hyperbolic-parabolic membrane structures. *Struct. Eng. Mech.* **2020**, *76*, 269–278. [CrossRef]

39. Wang, X.; Chu, H.; Yang, Q. Numerical Analysis of Wind-Induced Response of a Wrinkled Membrane. *Int. J. Struct. Stab. Dyn.* **2020**, *20*, 2050056. [CrossRef]
40. Zhang, L.; Ma, D.; Yang, M.; Yao, Y.; Yu, Y.; Yang, X. Experimental and Numerical Study on the Performance of Double Membrane Wing for Long-Endurance Low-Speed Aircraft. *Appl. Sci.* **2022**, *12*, 6765. [CrossRef]
41. Vizotto, I.; Ferreira, A.M. Wind force coefficients on hexagonal free form shell. *Eng. Struct.* **2015**, *83*, 17–29. [CrossRef]
42. Yu, N.G.; Chen, H.S.; Xu, Q.; Hasan, M.M.; Sie, O. Wafer map defect patterns classification based on a lightweight network and data augmentation. *CAAI Trans. Intell. Technol.* **2023**, *8*, 1029–1042. [CrossRef]
43. Chen, Z.S.; Zhang, L.K.; Li, K.; Xue, X.Y.; Zhang, X.L.; Kim, B.; Li, C.Y. Machine-learning prediction of aerodynamic damping for buildings and structures undergoing flow-induced vibrations. *J. Build. Eng.* **2023**, *63*, 105374. [CrossRef]
44. Jovanovic, N.M. Analyzing Wireless Mesh Network Using Spectral Graph Theory. *Artif. Intell. Appl.* **2022**. [CrossRef]
45. Luo, C. KELL: A Kernel-Embedded Local Learning for Data-Intensive Modeling. *Artif. Intell. Appl.* **2024**, *2*, 38–44. [CrossRef]
46. Zhou, C.L.; Shi, Q.; He, D.; Tu, B.; Li, H.Y.; Plaza, A. Spectral-spatial sequence characteristics-based convolutional transformer for hyperspectral change detection. *CAAI Trans. Intell. Technol.* **2023**, *8*, 1237–1257. [CrossRef]
47. Khan, J.; Lee, E.; Kim, K. A higher prediction accuracy-based alpha-beta filter algorithm using the feedforward artificial neural network. *CAAI Trans. Intell. Technol.* **2023**, *8*, 1124–1139. [CrossRef]
48. Yusuf, A.; Kiri, A.A.; Lawal, L.; Kiri, A.I. A Hybrid Conjugate Gradient Algorithm for Nonlinear System of Equations through Conjugacy Condition. *Artif. Intell. Appl.* **2022**. [CrossRef]
49. Zhou, X.; Han, Z.; Gu, M.; Zhang, A.; Zhang, W.; Fang, W. Research on wind-induced responses of a large-scale membrane structure. *Earthq. Eng. Eng. Vib.* **2013**, *12*, 297–305. [CrossRef]
50. Zhou, Y.; Li, Y.; Yoshida, A. Effect of Added Mass on Wind-Induced Vibration of a Circular Flat Membrane by Wind Tunnel Tests. *Int. J. Struct. Stab. Dyn.* **2018**, *18*, 1850156. [CrossRef]